Nanotechnology **18** (2007) 495704 (7pp) doi:10.1088/0957-4484/18/49/495704

Morphological tuning and conductivity of organic conductor nanowires

Huibiao Liu[1], Junbo Li[1], Changshi Lao[2], Changshui Huang[1], Yuliang Li[1], Zhong Lin Wang[2] and Daoben Zhu[1]

[1] CAS Key Laboratory of Organic Solid, Beijing National Laboratory for Molecular Sciences (BNLMS), Institute of Chemistry, Chinese Academy of Sciences, Beijing 100080, People's Republic of China
[2] School of Materials Science and Engineering, Georgia Institute of Technology, Atlanta, GA 30332-0245, USA

E-mail: ylli@iccas.ac.cn and zhong.wang@mse.gatech.edu

Received 21 September 2007
Published 2 November 2007
Online at stacks.iop.org/Nano/18/495704

Abstract
We report the synthesis of small-molecule organic conductor nanowires of TTF-TCNQ by selective inducement in a two-phase method by π–π stacking interaction. The morphologies of TTF-TCNQ, from straight nanowires to helical nanowires and to complicated helical dendrite structures, have been controlled by adjusting the experimental conditions. The technique has been applied to the synthesis of AgTCNQ/CuTCNQ nanowires in a two-phase system of acetonitrile/hexane. I–V characterization of an individual nanowire indicated that the conductivity along the b-axis of the TTF-TCNQ helical nanowire is much better than that along other directions. The synthetic procedure presented is a general approach for producing controlled organic conductor/semiconductor nanowires.

(Some figures in this article are in colour only in the electronic version)

1. Introduction

Recently, significant efforts have been devoted to fabricating hierarchical quasi-one-dimensional (1D) nanostructures, such as helix, coil, ring, spring, bow, and so on, owing to their attractive properties and morphologies [1–5]. Previous works in this area have highlighted the concept for synthesizing nanomaterials with helical nanostructures, but they are limited to inorganic [1–5] and polymeric materials [6] as well as peptides [7]. Chemical vapor deposition (CVD) [2b], the template technique [8], solid–vapor growth [9] and the self-assembly technique [7] are still general synthesis routes for synthesizing helical shaped nano- and micro-structures. All of these methods require high temperature and templates. For some applications, facile and template-free methods are highly desirable for preparation of helical nanostructures.

Small-molecule organic conductors and semiconductors have attracted much attention for more than three decades. These organic complexes have been identified to have potential applications in molecular electronic devices, optical switching and nonlinear optical devices [10]. As a well-known organic charge transfer (CT) salt, TTF-TCNQ (tetrathiafulvalene-7,7′,8,8′-tetracyanoquinodimethane) bulk crystal has been intensively studied [11] because of its quasi-one-dimensionality and high electronic conductivity (10^3 S cm^{-1}) along the b-axis of the single crystal. However, studies on the fabrication of nanostructures and properties at the nanoscale of the TTF-TCNQ CT complex are rare [12]. The objectives of some fundamental studies are to understand (a) if charge transfer can occur to form complex and morphology controlled nanostructures using TTF-TCNQ molecules and (b) how to exploit the properties of the charge transfer complex at the nanoscale. Therefore, developing new methods for synthesizing TTF-TCNQ CT complex materials on a nano- or micro-scale to extend their research fields is still a challenging task in materials chemistry.

As we know, the two-phase method was developed for synthesizing noble metal nanocrystals, such as Pt, Pd, Ag and Au [13], and extended to prepare semiconductor nanocrystals [14]. However, the fabrication of 1D nanomaterials using the two-phase method has not been reported. We now develop this approach to successfully

spatially separate the nucleation, growth and assembly of nanoparticles, which, in principle, provides a controlled synthesis approach to 1D nanomaterials and complex helical nanostructures. In this paper, we report the synthesis of small molecular organic conductor TTF-TCNQ helical nanowires by π–π stacking interaction using the two-phase method. Moreover, the morphologies of TTF-TCNQ—from a straight nanowire to a helical nanowire and to a complicated helical dendrite structure with uniform and monodispersivity—have been controlled by adjusting the experimental conditions. The current synthetic procedure is a general approach for producing organic conductor/semiconductor hierarchical one-dimensional nanostructures, such as CuTCNQ and AgTCNQ nanowires. The I–V characteristics of a single TTF-TCNQ helical nanowire have been measured. The result indicated that the conductivity along the b-axis of the TTF-TCNQ helical nanowire is much higher than that along other directions. Study of the complex of TTF and TCNQ molecules indicated that the charge transfer complex may be responsible for forming the nanostructures.

2. Experimental details

Synthesis of TTF-TCNQ

Tetrathiafulvalene and 7,7′,8,8′-tetracyanoquinodimethane was purchased from Alfa Aesar. Other chemical reagents used in the experiments were purchased from Beijing Chemical Reagent Co. Ltd, China. TTF-TCNQ CT salts with different morphologies were prepared using a two-phase method by adjusting the experiment conditions. Equation (1) shows the chemical reaction in our system:

$$\text{TTF (hexane)} + \text{TCNQ (acetonitrile)} \rightarrow \text{TTF-TCNQ (s)} \downarrow . \quad (1)$$

TTF solutions were prepared by dissolving TTF in hexane and TCNQ solutions were prepared by dissolving TCNQ in acetonitrile. To investigate the effect of the TCNQ concentration, four samples were prepared in the following steps: 10 ml solution of TCNQ in acetonitrile (0.03 M) was dripped into 10 ml TTF solution in hexane (0.025 M) at the rate of x μl s^{-1} with stirring, where x was 1, 20, 40, and 500, respectively. After TCNQ solution dripping, the solution continued to be stirred for 10 min. The samples obtained were centrifuged, washed three times with acetone and dried in ambient atmosphere. To investigate the effect of temperature, four samples were prepared using the same concentrations of TTF (0.025 M) and TCNQ solution (0.03 M). TCNQ solution was poured into TTF solution with stirring at different temperatures: −50, −10, 0 and 50 °C respectively.

Synthesis of CuTCNQ and AgTCNQ nanowires

Copper and silver nanoparticles were prepared according to references [15, 16]. The copper and silver nanoparticles prepared were separated by centrifugation and washed three times with ethanol. The following is a typical synthetic procedure for CuTCNQ and AgTCNQ nanowires: 60 mg of TCNQ solution in acetonitrile (20 ml) poured into 20 mg of the copper nanoparticles dispersed into hexane solution (20 ml) with stirring at room temperature and kept at room temperature for 30 min. The resulting solution containing the CuTCNQ nanowires is deep blue. The nanowires were separated by centrifugation, and washed with acetone and dried in ambient atmosphere to provide pure nanowires of complexes of CuTCNQ. The AgTCNQ nanowires were also prepared using similar procedures.

The x-ray diffractometer (XRD) patterns were recorded using a Japan Rigaku D/max-2500 rotating anode x-ray diffractometer equipped with graphite monochromatized Cu Kα radiation (λ = 1.541 78 Å), employing a scanning rate of 0.05° s^{-1} in the 2θ range from 5° to 50°. For SEM observation, the morphologies of the samples were studied using a JEOL JSM 6700F field-emission scanning electron microscope. The samples were suspended in ethanol and dispersed on Au-coated silicon chips previously mounted onto stainless-steel sample holders using two-sided carbon tape. Specimens for the TEM (Tecnai F30 microscope with a 200 kV accelerating voltage) and SAED patterns were dispersed in ethanol using ultrasound. A droplet of the suspension was placed on a holey copper grid covered with porous carbon film.

I–V transport measurements

With a dry transfer printing method, we aligned the TTF-TCNQ nanowires across two prefabricated Au electrodes. Then, we use a focused ion beam system, FEI Nova 200, to deposit Pt on the contact areas to improve the contact. With the preparation of the electrodes, the nanowire samples were tested in a home-built electrical measurement system, with a Cascade RFI probe system, a Stanford Research System DS345 signal generator and a DL Instrument 1211 current preamplifier.

3. Results and discussion

We employed acetonitrile and hexane as two liquid phases for synthesizing the organic conductor of TTF-TCNQ. The concentrations of the reactants were controlled by adjusting the drip rate of TCNQ solution in acetonitrile for tuning TTF-TCNQ morphologies. TTF-TCNQ nanowires were obtained when 10 ml solution of TCNQ in acetonitrile (0.03 M) was dripped into 10 ml TTF solution in hexane (0.025 M) at the rate of 1 μl s^{-1} with stirring. The scanning electron microscopy (SEM) image (figure 1(A)) shows that the diameter and length of the nanowires are 200–700 nm and above 10 μm, respectively. Increasing the drip rate to 20 μl s^{-1} facilitates the quickening rate of nucleation, growth and assembly, resulting in the formation of TTF-TCNQ helical nanowires (figure 1(B)), with diameters of 200–900 nm and lengths of several tens of micrometers. The helical angle with respect to the wire axis is schematically indicated in the corresponding nanowires, and ranges from 5° to 40°. Figure 1(C) presents some typical helical dendrites obtained at the drip rate of 40 μl s^{-1} TCNQ solution in acetonitrile. A straight stiff microwire is directly connected to the starting point of the helical dendrite, that consists of many helical nanowires. Although the helical nanowires can be left and right handed, the helical direction of nanowires in each branch of the helical dendrite is the same. The branches grow continuously on helical directions along the trunk to produce complicated helical dendrites. The complicated TTF-TCNQ helical dendrite (figure 1(D)) formed

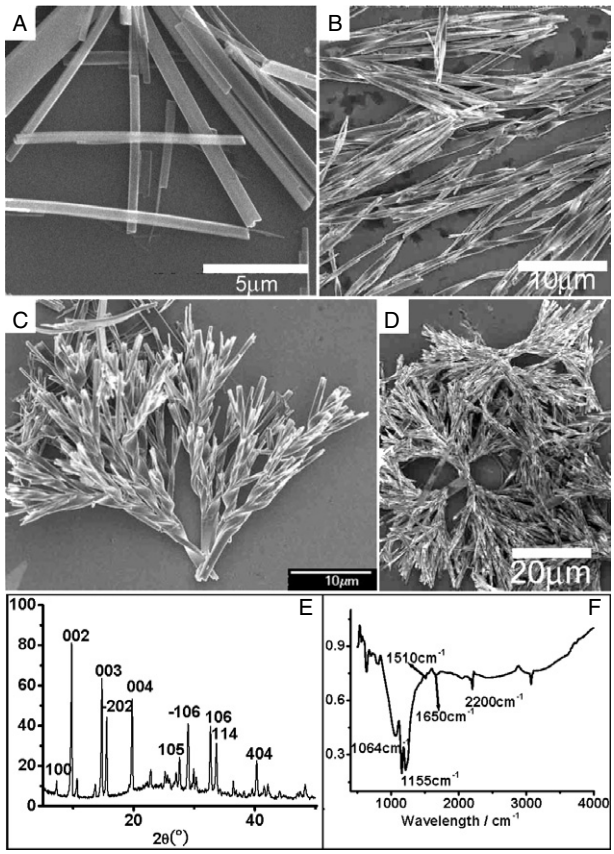

Figure 1. SEM images of TTF-TCNQ complex morphologies as prepared at the drip rate of (A) 1 μl s^{-1}, TTF-TCNQ nanowires; (B) 0.02 ml s^{-1}, TTF-TCNQ helical nanowires; (C) 0.04 ml s^{-1}, TTF-TCNQ helical dendrites; (D) 0.5 ml s^{-1}, TTF-TCNQ complicated helical dendrites. (E) XRD patterns of TTF-TCNQ helical nanowires. (F) FT-IR spectrum of TTF-TCNQ dendrite with helical nanowires.

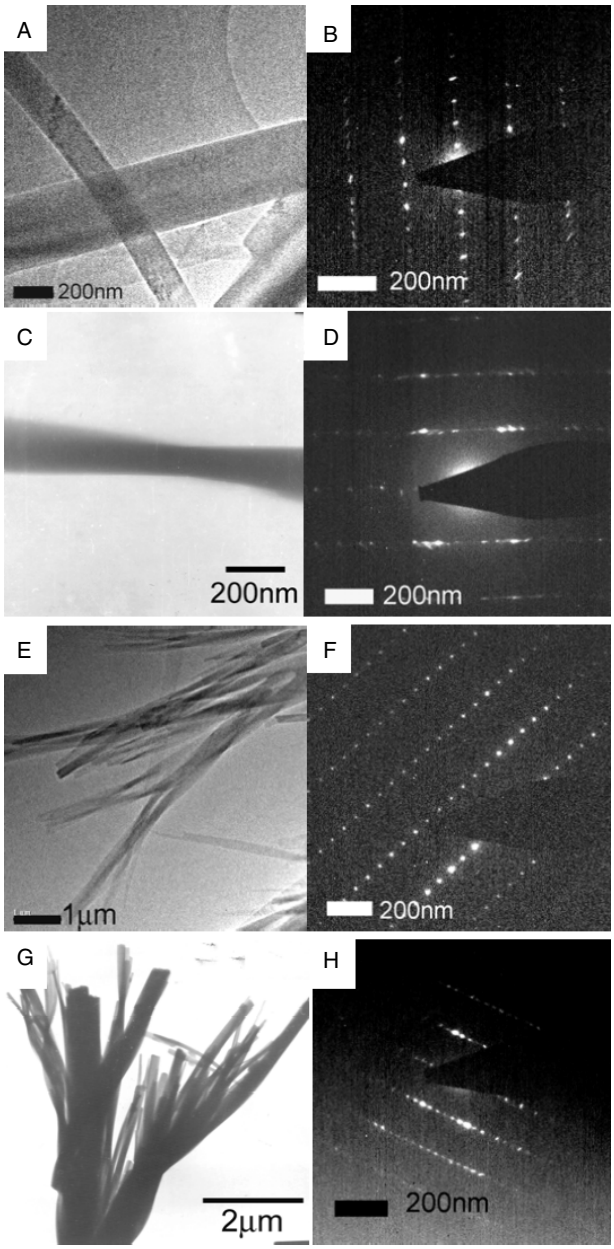

Figure 2. (A) TEM image of TTF-TCNQ nanowires. (B) SAED pattern of a TTF-TCNQ nanowire. (C) TEM image of a typical single TTF-TCNQ helical nanowire. (D) SAED pattern of a TTF-TCNQ helical nanowire. (E) TEM image of TTF-TCNQ helical dendrite. (F) SAED pattern of a TTF-TCNQ helical dendrite. (G) TEM image of a TTF-TCNQ complicated helical dendrite. (H) SAED pattern of a TTF-TCNQ complicated helical dendrite.

at the drip rate of 500 μl s^{-1}, is composed of two helical dendrites, connected with each other. Each helical dendrite is an assembly of many helical nanowires.

The TTF-TCNQ nanowires were characterized by FT-IR spectra (figure 1(F)), which provide evidence about bonding in the complex of TTF and TCNQ. The appearance of new bands at 1650 and 1145 cm^{-1} indicates the presence of benzenoid ring structure. The skeletal bands of the quinoid ring almost disappeared [17]. Figure 1(E) shows the x-ray diffraction (XRD) analyses of the TTF-TCNQ nanowires, which is attributed to monoclinic space group $P2_{1/C}$, and the sharp peaks imply high crystallinity and purity of the sample [18].

The morphology and structure of the TTF-TCNQ complex were further characterized by TEM and SAED. Figure 2(A) displays the TEM image of the obtained TTF-TCNQ nanowires with the diameter of 200–400 nm. The indexing of the spots in the SAED pattern (figure 2(B)) indicates that the TTF-TCNQ nanowires are single crystals. Figure 2(C) shows the TEM image of a typical TTF-TCNQ helical nanowire with a helical angle of about 15°. The SAED pattern (figure 2(D)) also demonstrates that the TTF-TCNQ helical nanowire is a single crystal. Figure 2(E) shows the TEM image of TTF-TCNQ dendrites with helical nanowires, whose diameters are in the range of 100–400 nm. As shown in figure 2(G), the TEM image of a typical TTF-TCNQ complicated helical dendrite is composed of many helical nanowires with diameter of 100–700 nm. Their SAED patterns (figures 2(F) and (H)) indicate that the TTF-TCNQ helical dendrites and complicated helical dendrites are single crystals as well.

The separation of the nucleation from the growth of monodisperse nanoparticles [19] by delayed nucleation [20] and surfactant-mediated growth [21, 22] has successfully

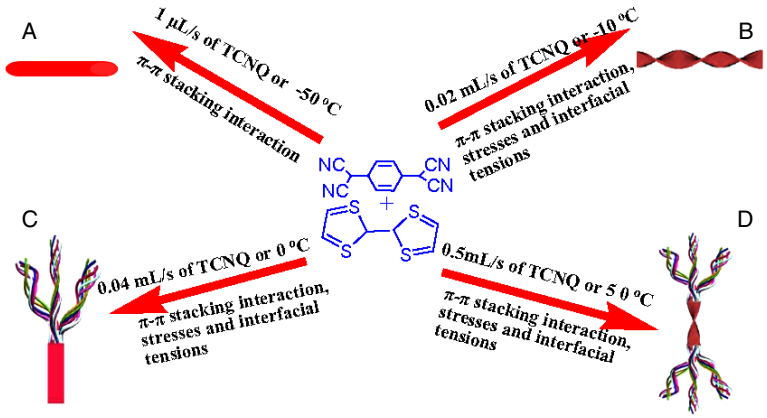

Scheme 1. Shape control of TTF-TCNQ nanostructures: (A) TTF-TCNQ nanowires; (B) TTF-TCNQ helical nanowires; (C) TTF-TCNQ helical dendrites; (D) TTF-TCNQ complicated helical dendrites.

been used for preparation of inorganic nanocrystals. The liquid–liquid interface can offer a unique alternative platform for spatially separating both the nucleation and growth of nanoparticles in organic materials. In the process, the nucleation and growth occurred at the interface of the two liquid phases, and the nuclei can subside into the bottom of the two phases when the nuclei are formed at the liquid–liquid interface, and the nanoparticles are unable to continuously grow at the bottom of the solution. The particles renew their growth when they are back to the interface by stirring control. Thus, the controlled size and shape can be achieved by precise manipulation of the nucleation and growth process. It is obviously different from the growth of inorganic nanomaterials; these organic supramolecular aggregates are formed through concerted weak interactions. Hydrogen bonding, π–π stacking, van der Waals forces and electrostatic interactions played central roles in controlling the structures and shapes of the aggregates. Therefore, the organic molecular systems are easier to aggregate to form complex nanostructures.

In our experiments, the assembly of TTF-TCNQ nanoparticles and the growth are simultaneous. The assembly of nanoparticles at the liquid–liquid interface is a highly dynamic process due to the strong interfacial tension [23]. Thereby, the assembly can be controlled by tuning the growth conditions. As shown in scheme 1, due to π–π stacking interactions between TTF molecules and TCNQ molecules, the TTF-TCNQ possesses a quasi-1D crystal structure along the *b*-axis [11]. The perfect directional π–π stacking interaction effectively increases the growth rate along *b*-axis. The faster growth rate along the *b*-axis is due to the π–π stacking interaction for inducing the formation of TTF-TCNQ nanowires (scheme 1 A). With increasing the drip rate of TCNQ solution, the concentration of the TCNQ solution in the TTF solution is enhanced, which increases the absolute growth rates of TTF-TCNQ and the assembly process in the system. The strain and interfacial tensions may be responsible for the wire twisting and formation of the TTF-TCNQ helical nanowire (scheme 1 B). A further increase in drip rate of TCNQ solution indicated faster growth and assembly rates of the TTF-TCNQ nanowires, possibly leading to the formation of helical dendrites (scheme 1 C), which can eventually evolve into complex helical dendrites (scheme 1 D).

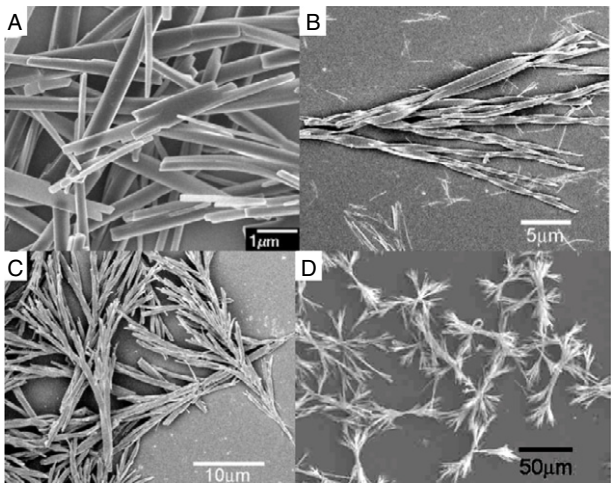

Figure 3. SEM images of TTF-TCNQ obtained under different reaction temperatures: (A) TTF-TCNQ nanowires at −50 °C; (B) TTF-TCNQ helical nanowires at −10 °C; (C) TTF-TCNQ helical dendrites at 0 °C; (D) TTF-TCNQ complicated helical dendrites at 50 °C.

The temperature and concentration of the reaction are two key factors for influencing the nucleation and growth. Under a low reaction temperature, the absolute growth rate of TTF-TCNQ is low. The π–π stacking interaction along the *b*-axis quickly forms nanowires. With increasing reaction temperature, the speeded up absolute growth rates of TTF-TCNQ may produce a large strain on the surface of nanowires, which is likely to result in the transformation of straight nanowires into helical nanowires, which may eventually evolve into complex growth patterns.

As we expected, the nanowires, helical nanowires and complicated helical dendrite structure of TTF-TCNQ are obtained under different reaction temperatures. When the reaction of TTF and TCNQ was kept in the lower temperature range of −50 °C, pouring TTF solution into TCNQ with stirring formed the TTF-TCNQ nanowires (figure 3(A)). The diameter and the length of TTF-TCNQ nanowires is in the

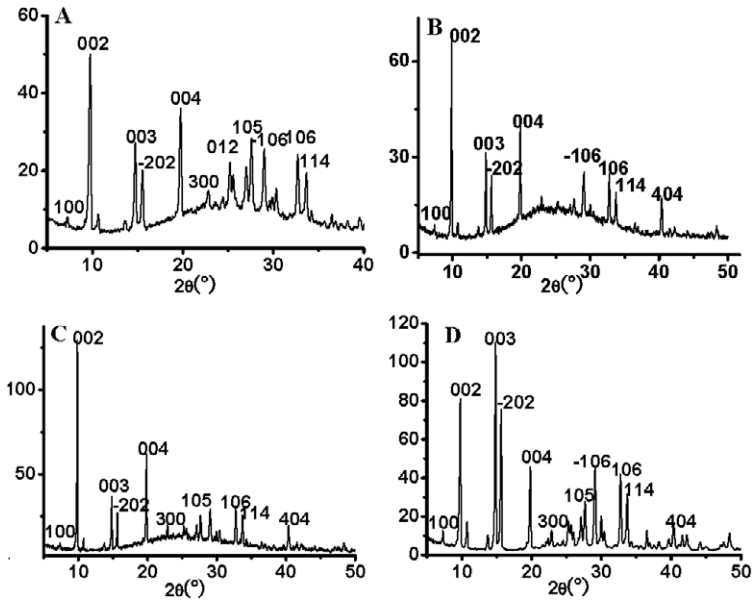

Figure 4. XRD pattern of TTF-TCNQ prepared under different reaction temperatures: (A) TTF-TCNQ nanowires at −50°C; (B) TTF-TCNQ helical nanowires at −10°C; (C) TTF-TCNQ helical dendrites at 0°C; (D) TTF-TCNQ complicated helical dendrites at 50 °C.

range of 100–500 nm and a few micrometers to tens of micrometers, respectively. When the reaction temperature was increased to −10 °C, the helical wires as shown in figure 3(B) were obtained, with a diameter of 300–800 nm and a length of 3–18 μm. Figure 3(B) shows that the helical angle ranges from 7 to 50°. The TTF-TCNQ helical dendrites (figure 3(C)) were produced at 0 °C, while the TTF-TCNQ complicated helical dendrites (figure 3(D)) were formed at 50 °C. Figure 4 shows the XRD analyses of the different shape of TTF-TCNQ complexes to be monoclinic space group $P2_{1/C}$, and the sharp peaks indicate high crystallinity [16].

We also used the method for fabricating AgTCNQ/Cu TCNQ nanowires through the reactions of silver/copper nanoparticles with TCNQ solution in two phases of acetonitrile/hexane, utilizing π–π stacking interaction between TCNQ inter-molecules (figure 5). The diameters of CuTCNQ nanowires are about 40–70 nm (figure 5(B)) and the diameters of AgTCNQ nanowires (figure 5(D)) are about 130–180 nm.

In order to quantify the anisotropic transport properties of the nanowires, the conductivities of individual nanowires have been measured. Because the TTF-TCNQ nanowires conduct only along the *b*-axis, we used two different configurations of electrodes to prove that the same conducting property is preserved in the nanowires. For devices in figure 6(A), the contacts are made at the side wall of the TTF-TCNQ nanowire with focused ion beam (FIB) Pt deposition. For devices made in this configuration, the conductivity is 3.8×10^{-4} S cm^{-1} when the bias voltage is below 1 V, and 1.05×10^{-2} S cm^{-1} when the bias voltage is above 4 V (figure 6(B)). For devices in figure 6(C), we firstly use FIB to mill an open cut at both ends of the TTF-TCNQ nanowire, then we deposit Pt on the open ends to connect the electrodes and nanowire together. For devices made in this way, the conductivity is 0.26 S cm^{-1} when the bias voltage is below 1 V and 295 S cm^{-1} when the bios voltage is above 4 V (figure 6(D)). We can see that

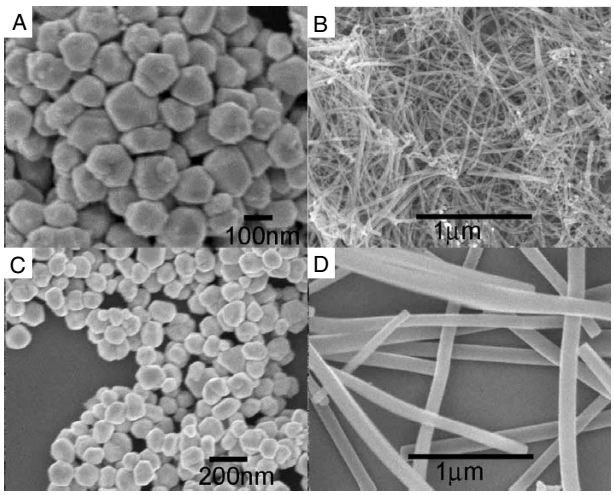

Figure 5. (A) Cu nanoparticles with diameters of about 60–130 nm. (B) CuTCNQ nanowires prepared by the two-phase method. (C) Ag nanoparticles with diameters of about 80–150 nm. (D) AgTCNQ nanowires prepared by the two-phase method.

the nanowire device in the second configuration displays much larger conductivity.

The *I*–*V* characteristic difference of these two types of samples comes from special carrier transport properties of the TTF-TCNQ nanowires. As reported in the literature [11], because of the high energy barrier between two different TTF-TCNQ columns, the TTF-TCNQ nanowire conducts only along the *b*-axis in a single TTF-TCNQ column [11]. As discussed in the previous section, the growth direction of these TTF-TCNQ nanowires is right along the *b*-axis. For the sample in figure 6(A), the contacts are made on the side wall of the TTF-TCNQ nanowire; in such a case, the carriers need to overcome the energy barrier between TTF-TCNQ columns for

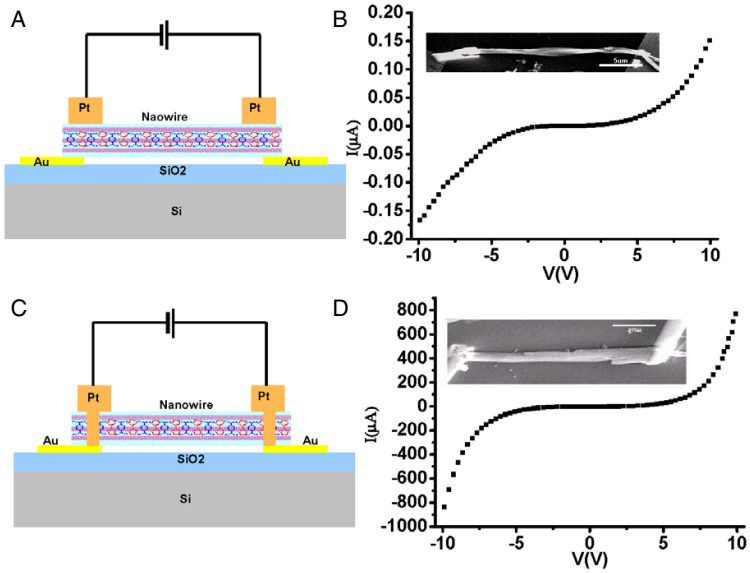

Figure 6. (A) Schematic diagram and SEM image of the device with contacts made on the side wall of the TTF-TCNQ helical nanowire; (B) the I–V characteristic of the corresponding nanowire in (A). (C) Schematic diagram and SEM image of the device with contacts made on the ends of the TTF-TCNQ helical nanowire (open ends were milled with FIB), (D) the I–V characteristic of the corresponding nanowire in (C).

current transport. So the conductance of the nanowire in this configuration is very small. However, when the bias voltage is greater than 4 V, the electrons can then tunnel through the energy barrier and the whole device become conducting and process higher conductance. For the sample in figure 6(B), the Pt electrodes made a direct contact with the TTF-TCNQ tunneling channel, so the conductance of the nanowire in this device is much higher. Above 4 V, when the bias voltage is high enough to make the tunneling across the columns possible, there are more conducting channels available. This accounts for the conductance increasing at above 4 V. This huge conductance difference between these two electrode configurations proved that the TTF-TCNQ nanowires conduct only along the *b*-axis in TTF-TCNQ columns.

4. Conclusions

Through π–π stacking interaction inducement using a facile liquid–liquid two-phase method, this paper presents a novel fabrication of self-assembly from a simple straight nanowire to a helical nanowire to a hierarchically complex helical dendrite of organic conductor TTF-TCNQ. I–V measurements of an individual nanowire indicated that the TTF-TCNQ helical nanowire is conducting along the *b*-axis, with a conductivity of $\sim$295 S cm^{-1}. The approach demonstrated in this paper is able to control the nucleation, growth and assembly in the liquid–liquid two-phase system, and is a generalized process that can be used to synthesize different kinds of organic conductor/semiconductor nanowires, which should have an outstanding potential for ordered nano- and microscale architectures for advanced devices.

Acknowledgments

This work was supported by the National Nature Science Foundation of China (20531060, 20473102 and 20571078) and the National Basic Research 973 Program of China (grant Nos 2006CB932100 and 2005CB623602). CSL and ZLW thank US NSF, DARPA and NIH (CCNE) for support.

References

[1a] Gao P X, Ding Y, Mai W, Hughes W L, Lao C and Wang Z L 2005 *Science* **309** 1700
[1b] Bae S Y, Lee J, Jung H, Park J and Ahn J P 2005 *J. Am. Chem. Soc.* **127** 10802
[2] Amelinckx S, Zhang X B, Bernaerts D, Zhang X F, Ivanov V and Nagy J B 1994 *Science* **265** 635
[3] Kong X Y, Ding Y, Yang R and Wang Z L 2004 *Science* **303** 1348
[4] Kong X Y, Ding Y, Yang R and Wang Z L 2004 *Nano Lett.* **4** 1309
[5a] Hughes W L and Wang Z L 2004 *J. Am. Chem. Soc.* **126** 6703
[5b] Tang Y H, Zhang Y F, Wang N, Lee C S, Han X D, Bello I and Lee S T 2001 *J. Appl. Phys.* **85** 7981
[6] Song J, Cheng Q, Kopta S and Stevens R C 2001 *J. Am. Chem. Soc.* **123** 3205
[7] Wanger D E, Phillips C L, Ali W M, Nybakken G E, Crawtord E D, Schwab A D, Smith W F and Fairman R 2005 *Proc. Natl Acad. Sci.* **102** 12656
[8] Yu S, Colfen H, Tauer K and Antonietti M 2005 *Nat. Mater.* **4** 51
[9] Lilach Y, Zhang J, Moskovits M and Kolmakov A 2005 *Nano Lett.* **5** 2019
[10a] Musa D, Munindrasdasa A I, Amaratunga G A J and Eccleston W 1998 *Nature* **395** 362
[10b] Spatz J P 2002 *Angew. Chem. Int. Edn* **41** 3359
[10c] Chiu J J, Kei C C, Perng T P and Wang W S 2003 *Adv. Mater.* **16** 1361
[10d] Liu H B *et al* 2005 *J. Am. Chem. Soc.* **127** 1120
[11] Jerome D 2004 *Chem. Rev.* **104** 5565
[12a] Sakai M, Iizuka M, Nakamura M and Kudo K 2003 *Japan. J. Appl. Phys.* 1 **142** 2488
[12b] de Caro D, Sakah J, Basso-Bert M, Faulmann C, Legros J P, Ondarcuhu T, Joachim C, Aries L, Valade L and Compt C P 2000 *Rend. Acad. Sci.* II **3** 675
[12c] Savy J P *et al* 2007 *New J. Chem.* **31** 519

[13] Brust M, Walker M, Bethell D, Schiffrin D J and Whyman R 1994 *J. Chem. Soc. Chem. Commun.* **7** 801
[14a] Pan D C, Jiang S C, An L J and Jiang B Z 2004 *Adv. Mater.* **16** 982
[14b] Wang Q, Pan D C, Jiang S C, Ji X L, An L J and Jiang B Z 2005 *Chem. Eur. J.* **11** 3843
[14c] Pan D C, Wang Q, Jiang S C, Ji X L and An L J 2005 *Adv. Mater.* **17** 176
[14d] Pan D C, Zhao N, Wang Q, Jiang S C, Ji X L and An L J 2005 *Adv. Mater.* **17** 1991
[14e] Zhao N, Pan D, Nie W and Ji X 2006 *J. Am. Chem. Soc.* **128** 10118
[15] Ren X, Chen D and Tang F S 2005 *J. Phys. Chem.* B **109** 15803
[16] Yamamoto M and Nakamoto M 2003 *J. Mater. Chem.* **13** 2064
[17a] Luneli B 1970 *J. Chem. Phys.* **52** 2375
[17b] Goswami D P and Kalra M L 1994 *J. Cryst. Growth* **135** 196
[18] Kistenmacher T J, Phillips T E and Cowan D O 1974 *Acta Crystallogr.* B **30** 763
[19] Xia Y, Yang P, Sun Y, Wu Y, Mayers B G, Yin Y, Kim F and Yan H 2003 *Adv. Mater.* **15** 353
[20] Casula M F, Jun Y W, Zaziski D J, Chan E M, Corrias A and Alivisatos A P 2006 *J. Am. Chem. Soc.* **128** 1675
[21] Murray C B, Norris D J and Bawendi M G 1993 *J. Am. Chem. Soc.* **115** 8706
[22] Yin Y and Alivisatos A P 2005 *Nature* **437** 664
[23] Binks B P and Lumsdon S O 2000 *Langmuir* **16** 8622